Parallel Channel Estimation for RIS-Assisted Internet of Things

Zhen Chen, *Senior Member, IEEE*, Lei Huang, *Senior Member, IEEE*, Shuqiang Xia, Boyi Tang, *Student Member, IEEE*, Martin Haardt, *Fellow, IEEE*, and Xiu Yin Zhang, *Fellow, IEEE*

***Abstract*— Reconfigurable intelligent surfaces (RISs) are deemed as a potential technique for the future of the Internet of Things (IoT) due to their capability of smartly reconfiguring the wireless propagation environment using a large number of low-cost passive elements. To benefit from RIS technology, the problem of RIS-assisted channel state information (CSI) acquisition needs to be carefully considered. Existing channel estimation methods usually ignored the different channel characteristics of direct channel and reflected channels. In fact, the reflected channel can be smartly configured by adjusting the phase shifts of the RIS, which is different from the direct channel due to the different path loss exponents between the transmitter and receiver. Therefore, it is necessary to further develop a RIS-assisted channel estimation to determine the direct and reflected channels, respectively. In this paper, we study a RIS-assisted channel estimation that jointly exploits the properties of the direct and the reflected channel to provide more accurate CSI. The direct channel is estimated using weighted ℓ_1 norm minimization, while the reflected channel is modeled based upon the robust $\ell_{1,\tau}$ norm minimization to sequentially estimate the channel parameters. Moreover, by combining the gradient descent and the alternating minimization method, a flexible and fast algorithm is developed to provide a feasible solution. Simulation results demonstrate that an RIS-aided MIMO system significantly reduces the active antennas/RF chains compared to other benchmark schemes.**

***Index Terms*— Channel estimation, compressed sensing, reconfigurable intelligent surface, mmWave MIMO.**

Manuscript received 23 December 2022; revised 30 July 2023 and 23 November 2023; accepted 5 February 2024. This work was supported in part by the National Natural Science Foundation of China under Grant 62001171 and Grant 62371197; in part by the National Science Fund for Distinguished Young Scholars under Grant 61925108; in part by the Key Project of International Cooperation and Exchanges of the National Natural Science Foundation of China under Grant 62220106009; in part by the Natural Science Foundation of Guangdong Province under Grant 2022A1515011189; in part by the Open Research Fund of National Mobile Communications Research Laboratory, Southeast University, under Grant K202411; in part by the Project of Shenzhen Peacock Plan Teams under Grant KQTD20210811090051046; and in part by the Shenzhen University 2035 Program for Excellent Research. The Associate Editor for this article was M. A. Khan. *(Corresponding author: Lei Huang.)*

Zhen Chen is with the School of Electronic and Information Engineering, South China University of Technology, Guangzhou 510640, China, and also with the National Mobile Communications Research Laboratory, Southeast University, Nanjing 211189, China (e-mail: chenz.scut@gmail.com).

Lei Huang is with the State Key Laboratory of Radio Frequency Heterogeneous Integration, Shenzhen University, Shenzhen 518060, China (e-mail: lhuang@szu.edu.cn).

Shuqiang Xia is with ZTE Corporation, Shenzhen 518055, China, and also with the State Key Laboratory of Mobile Network and Mobile Multimedia Technology, Shenzhen 518055, China (e-mail: xia.shuqiang@zte.com.cn).

Boyi Tang is with the Department of Electronic and Electrical Engineering, University College London, WC1E 6BT London, U.K. (e-mail: tangboyi_2000@163.com).

Martin Haardt is with the Communications Research Laboratory, Ilmenau University of Technology, 98684 Ilmenau, Germany (e-mail: martin.haardt@tu-ilmenau.de).

Xiu Yin Zhang is with the School of Electronic and Information Engineering, South China University of Technology, Guangzhou 510640, China (e-mail: zhangxiuyin@scut.edu.cn).

Digital Object Identifier 10.1109/TITS.2024.3364248

I. Introduction

IN THE era of the Internet of Things (IoT), a large physical size of antenna arrays has significantly improved the rate of wireless networks to serve multiple single-antenna IoT devices simultaneously [1]. To support massive connectivity and meet the requirement of huge data transmission demands, massive multiple-input-multiple-output (MIMO) is a key enabling technology for the IoT systems. However, a massive number of antenna arrays at the base station (BS) leads to high hardware costs and power consumption. It will inevitably aggravates the coverage issue for IoT communications [2]. To tackle these challenges, reconfigurable intelligent surfaces (RISs) have lately gained increasing interest as a candidate technology to enhance the spectral efficiency (SE) of fifth generation (5G) networks [3]. An RIS is generally composed of a large number of hardware-efficient passive elements [4], [5], e.g., phase shifters, which can dynamically modify the propagation direction of the incident signal by adjusting its phase shifters, and effectively improve the propagation environment with almost negligible power consumption. It is worth mentioning that RISs can also be utilized to bypass some barriers on the channel, or avoid the signal to be monitored. Due to its cost-effective, low-cost hardware and ease of placing, RISs have been recognized as one of the key enablers of the IoT vision, which has become a hot spot in the field of communications.

It was observed that existing cellular standards, including 4G LTE, are unable to support massive IoT devices connectivity. Furthermore, an acquisition of the channel state information (CSI) is needed for effective transmissions. This will give rise to huge overheads, and thus will make IoT communications even more challenging. Moreover, compared with cellular networks, there are some new characteristics in RIS-assisted massive MIMO IoT systems, which include low latency [6], massive connectivity [7], physical layer security [8], and so on. Among them, the massive connectivity is caused by the large number of IoT devices. This massive connectivity characteristic necessitates much more channel accessing than that of cellular networks and thus, results in

a huge consumption in channel estimation overhead. On the other hand, the promising gains brought by RISs critically depend on the accuracy of the acquired CSI that plays a crucial role in determining the error performance and the capacity, due to the large number of channel coefficients associated with the reflecting elements of an RIS [9].

Considering that CSI is essential to RIS-assisted IoT applications, e.g., sensor data transmission, it is of great significance to study channel estimation in RIS-assisted massive MIMO IoT systems. There have been attempts to achieve more accurate channel estimation [10], [11], [12]. In [13], the authors developed a machine learning (ML)-based channel estimation concept. In [14], by taking advantages of hybrid evolutionary algorithm, a compressed sensing (CS)-based channel estimator was derived for RIS-assisted system, which can improve significantly the performance of channel estimation. Also, in [15], a low-complexity passive beamforming design for distributed RIS systems was proposed. However, satisfactory estimation result can only be achieved with large antenna arrays, which limits the approach in practical applications. By utilizing the CS-based dictionary learning method, a two-stage channel was estimated for RIS-assisted time-division duplexing system [16]. Most recent works considered an ideal RIS which has a uniform response, such as, the authors in [17] considered an RIS-assisted time-varying reflection model for orthogonal frequency division multiplexing (OFDM) system, where low-resolution phase shifters were employed in practical RISs. To reduce the training overhead, the works in [18] considered the semi-passive elements-aided channel estimation framework by exploiting the channel coherence time differences. After that, a three phase channel estimation scheme was developed, which improve the accuracy of estimation [19]. By leveraging the deficient structure of the RIS channels, practical residual neural networks were proposed to improve the RIS-assisted channel estimation accuracy [20]. In [21], a control protocol enabling linear square estimation was presented for the multiple-input single-output (MISO) channel. According to this protocol, partial elements of RISs were activated for maximizing downlink received power. Moreover, a scalar ambiguity estimation method based on maximum likelihood (ML) was recently exploited for blind channel estimation [22]. Considering the characteristics of the angles of departure/arrival (AoDs/AoAs), the atomic norm minimization was conducted to achieve the angular parameters and angle differences estimation [23]. The authors in [24] designed a minimum variance unbiased estimator for optimal channel estimation, in which the elements of RISs followed an optimal series of activation patterns. More recently, a joint channel training and RISs reflection coefficient optimization framework was investigated by maximizing the achievable rate of massive MIMO systems [25]. To mitigate the excessive pilot signaling overhead, a RIS-assisted codebook design with learning mechanism was developed to be more suitable for ultra-dense network [26]. In addition, time-varying Ricean fading channels were considered to RIS-aided high-mobility system design that providing reliable coverage [27]. More recently, RIS is considered to jointly optimize problem of the transmit precoding matrix of dual functional radar and communication (DFRC), the amplification matrix and the phase shift matrix of the active RIS [28]. Furthermore, the authors in [29] considered a trade-off design between communication and radar for RIS-Assisted DFRC System.

To exploit the sparse structure of the RIS channel in practical systems, such a sparse channel model is attracting more and more attention. The introduction of CS attracted an additional interest in RIS-assisted channel estimation and then the corresponding phase shift optimization schemes and algorithms were proposed [30], [31], [32], [33]. By exploring the properties of Kronecker products and the sparsity of the RIS channel, the cascaded channel estimation was formulated as a sparse signal recovery problem [34], and then a hybrid-based multiobjective optimization algorithm was exploited to determine the cascade millimeter wave (mmWave) channel. In [35], the authors combine CS and deep neural networks to reduce the pilot overhead of channel estimation by maximizing the achievable sum-rate of the system. In [36], the majorization-minimization-based algorithm was developed to estimate RIS channels, which performs better than least-squares (LS) approach. By virtue of the advantages of deep learning (DL), a deep denoising-based neural network framework was proposed to improve the effectiveness of channel estimation [37]. To reduce the estimation delay, the authors utilize CS and offset learning, recovering the RIS-assisted channel with a few pilot symbols [38]. On the basis of this analysis, DL-aided residual learning was exploited to tackle the intractable channel optimization problem [39]. In addition, considering the incident sign affect, an DL-based channel estimation algorithm was investigated to suppress this useless signal [33]. It is worth mentioning that the CS-based method usually involves complex mathematical problems as well as non-convex cost function due to the underdetermined sampling constraints. The DL-based channel estimation can overcome this issue, but needs the prerequisite of a large number of training samples.

To the best of our knowledge, the above-mentioned works on channel estimation are limited to hybrid RIS-assisted channels, in which the direct and the reflected channels are estimated together. However, the reflected channel is different from the direct channel due to the different path loss exponents between the direct and the reflected paths. Thus, they are inapplicable to practical IoT scenarios. This motivates us to put forward a RIS-assisted joint sparse channel estimation for the mmWave MIMO systems by exploiting the properties of the reflected and direct channels. To reduce the training time, a joint channel estimator of the weighted ℓ_1 and $\ell_{1,\tau}$ norm is developed by exploiting CS theory. To facilitate the performance improvement, an alternate iteration algorithm is proposed to estimate the direct and reflected channels, respectively. Simulation results verify the performance of the proposed scheme in accordance with the results of numerical calculation. The main contributions of this paper can be summarized as follows:

- We propose the parallel RIS-assisted channel estimation scheme, which can estimate the direct and reflected

channels separately. In the proposed channel estimation framework, the weighted ℓ_1 norm minimization is developed to obtain a better direct channel estimation solution. It is due to the fact that a properly reweighted ℓ_1 norm approximates the ℓ_0-pseudo-norm, which actually needs to be minimized, better than the standard ℓ_1 norm. On the other hand, considering the fact that the characteristic of the reflected channel is generally different from the direct channel, the robust $\ell_{1,\tau}$ norm minimization model is exploited to refine more accurate CSI, which can capture the changes of the channel condition in real time.

- To reduce the training overhead of the channel estimation solution, a flexible and fast optimization tool is developed by combining gradient descent and the alternating minimization method. As a consequence, the proposed approach is able to yield an approximate close-form solution, ending up with an efficient iterative implementation. Furthermore, an adaptive strategy is employed to determine the reasonable parameter in each iteration.
- To verify the theoretical result of the proposed scheme, the corresponding mean squared error (MSE) and error vector magnitude (EVM) for channel estimation are introduced to evaluate the performance of the proposed framework. In comparison to various benchmarks, numerical results confirm the superiority and accuracy of the proposed method, which is more suitable for RIS-assisted IoT systems, in particular in the high signal-to-noise ratio (SNR) regime.

A. Organization and Notation

The remainder of this paper is organized as follows. Section II presents an RIS-assisted system model along with the channel estimation problem, while Section III proposes the basic idea and provides the details about the proposed optimization procedure based on an alternate iteration algorithm. In Section IV, the theoretical findings are validated including comprehensive simulation results and assessments. Section V draws the conclusions we discuss the potential directions for future investigation.

Notation: Lower case bold faced and upper case bold faced letters are used to denote vectors and matrices, respectively. For a vector $\boldsymbol{a}$, $(\boldsymbol{a})^T$, and $(\boldsymbol{a})^H$ refer to the transpose, and the conjugate transpose, respectively; diag$(\cdot)$ is the diagonalization operation. Moreover, tanh$(\cdot)$ and cosh$(\cdot)$ denote hyperbolic tangent and hyperbolic cosine function, respectively. The Euclidean norm of a complex vector is denoted by $\|\cdot\|$, arctanh$(\cdot)$ is the inverse hyperbolic tangent function, $\nabla_{\boldsymbol{a}} f(\boldsymbol{a})$ represents the gradient vector with respect to $\boldsymbol{a}$, and $|\cdot|$ denotes the absolute value of a complex scalar. The symbol $\otimes$ stands for the Kronecker product operator.

II. System Model

We introduce a RIS-assisted mmWave MIMO system as shown in Fig. 1, where a RIS with N_{RIS} reflecting elements is modeled by a uniform planar array (UPA) that is deployed to assist communucation. The BS equipped with N_{BS} antennas to serve N_{UE} antennas of the user. We define $\boldsymbol{H}_{BU} \in \mathbb{C}^{N_{UE}\times N_{BS}}$

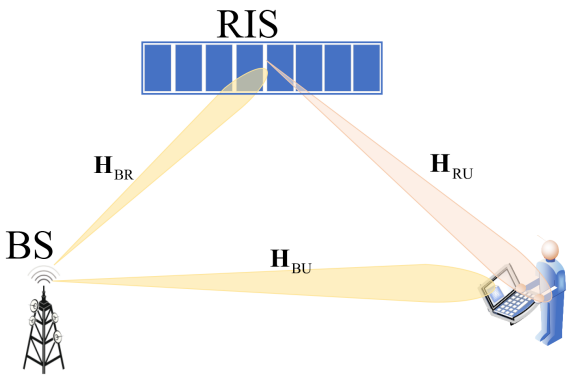

Fig. 1. The RIS-assisted downlink mmWave MIMO system.

as the direct channel from the BS to the user link. For RIS-assisted mmWave MIMO systems, we usually have $N_p < N_{BS}$ due to the large number of transmit antennas N_{BS} and the limited number of pilots N_p. We also consider a limited number of reflecting elements N_{RIS}, which is also larger than the number of pilots N_p. It is worth noting that the channel estimation scheme can be implemented at the transceiver, without any operation or algorithm needs to be executed at the RIS.

As shown in Fig. 1, the channel $\boldsymbol{H}$ consists of a direct channel and reflected channels, which is given by

$$\begin{aligned}\boldsymbol{H} &= \boldsymbol{H}_{BRU} + \boldsymbol{H}_{BU} \\ &= \underbrace{\boldsymbol{H}_{BR}\boldsymbol{\Phi}\boldsymbol{H}_{RU}}_{\text{reflected channels}} + \underbrace{\boldsymbol{H}_{BU}}_{\text{direct channels}}, \end{aligned} \tag{1}$$

where $\boldsymbol{H}_{BRU} \in \mathbb{C}^{N_{UE}\times N_{BS}}$ denotes the channel frequency response of the BS-RIS-user cascade channel. Here, $\boldsymbol{H}_{BR}$ and $\boldsymbol{H}_{RU}$ denote the channel matrix associated with the BS-RIS channel, and the channel matrix between the RIS and user, respectively. Then, the operation of the RIS is described by the diagonal matrix $\boldsymbol{\Phi} = \text{diag}\{\varphi_1, \ldots, \varphi_{N_{RIS}}\}$. To study a generalized model, first we assume $\mathcal{F}_1$ is the ideal RIS case, i.e., both the amplitudes and phase shifts of φ_i associated with the reflecting elements can be controlled independently and continuously [40], i.e.,

$$\mathcal{F}_1 \triangleq \{\varphi_i \,||\varphi_i\,| \leq 1\},\ i = 1, \ldots, N_{RIS} \tag{2}$$

However, the RISs are limited by the hardware implementation of metamaterials in practice. Therefore, non-ideal RIS cases should be considered. Based on this, we define the $\mathcal{F}_2$ as the general case, where only the phase of φ_i can be controlled continuously, and we also define the $\mathcal{F}_3$ as the discrete case, where the low-resolution phase of φ_i corresponds to discrete phase shifts, i.e.,

$$\mathcal{F}_2 \triangleq \{\varphi_i \,||\varphi_i\,| = 1\}, \tag{3a}$$

$$\mathcal{F}_3 \triangleq \left\{\varphi_i \mid \varphi_i \in \left\{1, e^{j\frac{2\pi}{L}}, \ldots, e^{j\frac{2\pi(L-1)}{L}}\right\}\right\}, \tag{3b}$$

where L indicates that $\mathcal{F}_3$ contains L discrete phase shifts [41].

By exploiting the sparse scattering characteristics of mmWave channels, the optimization problem can be formulated as a sparse recovery problem (e.g., [42], [43]). More specifically, the channel estimation problem of interest

involves finding a sparse geometric channel model, which is expressed as follows

$$\boldsymbol{H}_{BU} = \sum_{l=1}^{\tilde{L}_{BU}} \alpha_l \boldsymbol{\alpha}_{BS}(\theta_{BS,l}) \boldsymbol{\alpha}_{UE}^H(\theta_{UE,l}), \tag{4a}$$

$$\boldsymbol{H}_{BR} = \sum_{l=1}^{\tilde{L}_{BR}} \beta_l \boldsymbol{\alpha}_{BS}(\phi_{BR,l}) \boldsymbol{\alpha}_{RIS}^H(\phi_{RIS_1,l}), \tag{4b}$$

$$\boldsymbol{H}_{RU} = \sum_{l=1}^{\tilde{L}_{RU}} \delta_l \boldsymbol{\alpha}_{RIS}(\psi_{RIS_2,l}) \boldsymbol{\alpha}_{UE}^H(\psi_{RE,l}), \tag{4c}$$

where $\tilde{L}_{BU}$, $\tilde{L}_{BR}$ and $\tilde{L}_{RU}$ are the number of BS-UE, BS-RIS and RIS-UE paths, respectively. θ_l, $\phi_l \in [0, 2\pi]$ are the associated AoD and AoA, and $\boldsymbol{\alpha}_{BS} \in \mathbb{C}^{N_{BS}}$ ($\boldsymbol{\alpha}_{UE} \in \mathbb{C}^{N_{UE}}$, $\boldsymbol{\alpha}_{RIS} \in \mathbb{C}^{N_{RIS}}$) are the array response vectors associated with the BS, UE, and RIS, respectively.

Moreover, $\alpha_l = \tilde{\alpha}_l \sqrt{G(\theta_l) L(d_{BS})}$, $\beta_l = \tilde{\beta}_l \sqrt{G(\varphi_l) L(d_{RIS})}$ and $\delta_l = \tilde{\delta}_l \sqrt{G(\theta_l) L(d_{UE})}$; $\tilde{\alpha}_l$, $\tilde{\beta}_l$ and $\tilde{\delta}_l$ are the complex gain of the lth path, $G(\theta_l)$, $G(\varphi_l)$ and $G(\theta_l)$ are directional beamforming antenna arrays that are deployed to compensate the significant path-loss in the considered system. Thus, the antenna pattern of users can be approximated by a sectored antenna model in [44] which is given by

$$G(\Xi_l) = \begin{cases} \mathcal{G}, & \text{if } |\Xi_l| \le \theta_c \\ g, & \text{otherwise.} \end{cases} \tag{5}$$

where $\Xi_l = \{\theta_l, \varphi_l, \phi_l\}$, distributed in $[0, 2\pi]$, is the angle between the BS and the user, between the BS and the RIS, between the RIS and the user, respectively. θ_c denotes the beamwidth of the main lobe, $\mathcal{G}$ and g are respectively the array gains of main and sidelobes. $L(d_{BS})$, $L(d_{RIS})$ and $L(d_{UE})$ refer to the pathloss, which divided into two scenario.

For the first communication scenario without a RIS, different path loss equations are applied to model the LoS and NLoS links as [45]

$$L(d) = \begin{cases} d^{-\varsigma_i}, & \text{if BS} - \text{UE is LOS link} \\ d^{-\varsigma_{ii}}, & \text{if BS} - \text{UE is NLOS link.} \end{cases} \tag{6}$$

where ς_i and ς_{ii} are the LoS and NLoS path loss exponents, respectively.

For the second communication scenario with the assistance by the RIS, recently, the free-space path loss models of RIS-aided wireless communications are developed for different situations in [46]. Thus, we obtain

$$L(d_{BU}, d_{BRU}) = C_{BU} C_{BRU} d_{BU}^{-2} d_{BRU}^{-2}, \tag{7}$$

where C_{BU} and C_{BRU} denote the path loss intercepts of BS-RIS and RIS-user links, respectively.

To formulate the channel estimation as a sparse signal recovery problem, a beamspace MIMO representation of the direct channel for the RIS-assisted system is expressed as

$$\boldsymbol{H}_{BU} = \mathbf{A}_{BS} \boldsymbol{H}_\alpha \mathbf{A}_{UE}^H, \tag{8}$$

where $\mathbf{A}_{BS} \in \mathbb{C}^{N_{BS} \times \tilde{L}}$ is the array manifolds of BS, which has $\tilde{L}$ column vectors of dimension N_{BS}. $\mathbf{A}_{UE} \in \mathbb{C}^{N_{UE} \times \tilde{L}}$ is the array manifolds of user, which has $\tilde{L}$ column vectors of dimension N_{UE}. The array manifold in the horizontal and vertical directions can be formulated as

$$\mathbf{A}_{BS} \triangleq [\boldsymbol{\alpha}_{BS}(\theta_{BS,1}), \ldots, \boldsymbol{\alpha}_{BS}(\theta_{BS,\tilde{L}})], \tag{9a}$$

$$\mathbf{A}_{UE} \triangleq [\boldsymbol{\alpha}_{UE}(\theta_{UE,1}), \ldots, \boldsymbol{\alpha}_{UE}(\theta_{UE,\tilde{L}})] \tag{9b}$$

and $\boldsymbol{H}_\alpha \in \mathbb{C}^{\tilde{L} \times \tilde{L}}$ is the angular domain sparse matrix with $\tilde{L}$ non-zero entries corresponding to the channel gains $\{\alpha_l\}$.

Due to the limited scattering nature and small angular spreads, the number of non-zero entries of the sparse matrix $\boldsymbol{H}_\alpha$ is less than L, i.e., $\tilde{L} < L$. Similarly, the BS-RIS channel and the RIS-user channel are defined as

$$\boldsymbol{H}_{BR} = \mathbf{A}_{BR} \boldsymbol{H}_\beta \mathbf{A}_{RIS_1}^H, \tag{10a}$$

$$\boldsymbol{H}_{RU} = \mathbf{A}_{RIS_2} \boldsymbol{H}_\delta \mathbf{A}_{RE}^H, \tag{10b}$$

where $\mathbf{A}_{BR} \triangleq [\boldsymbol{\alpha}_{BS}(\phi_{BR,1}), \ldots, \boldsymbol{\alpha}_{BS}(\phi_{BR,L_{BR}})]$ that has L_{BR} column vectors of dimension N_{BS}. $\mathbf{A}_{RE} \triangleq [\boldsymbol{\alpha}_{UE}(\phi_{RE,1}), \ldots, \boldsymbol{\alpha}_{RE}(\phi_{RE,L_{RU}})]$ that has L_{RIS} column vectors of dimension N_{UE}. $\mathbf{A}_{RIS_1} \triangleq [\boldsymbol{\alpha}_{RIS}(\phi_{RIS,1}), \ldots, \boldsymbol{\alpha}_{RIS}(\phi_{RIS,L_{BR}})]$ that has L_{BR} column vectors of dimension N_{RIS}. $\mathbf{A}_{RIS_2} \triangleq [\boldsymbol{\alpha}_{RIS}(\psi_{RIS,1}), \ldots, \boldsymbol{\alpha}_{RIS}(\psi_{RIS,L_{BR}})]$ that has L_{RIS} column vectors of dimension N_{RIS}. $\boldsymbol{H}_\beta \in \mathbb{C}^{L_{BR} \times L_{BR}}$ and $\boldsymbol{H}_\delta \in \mathbb{C}^{L_{RIS} \times L_{RIS}}$ are sparse matrices corresponding to the transmission path gains $\{\beta_l\}_{l=1}^{L_{BR}}$ and $\{\delta_l\}_{l=1}^{L_{RIS}}$, respectively, when all channel parameters lie in the array response matrices.

Due to the sparse scattering characteristics of RIS-assisted systems, the beamspace channel matrices $\boldsymbol{H}_\beta$ and $\boldsymbol{H}_\delta$ are sparse matrices with a few non-zero entries. Suppose any sparse matrix in $\{\boldsymbol{H}_\beta, \boldsymbol{H}_\delta\}$ contains at most N_p nonzero entries, we usually have $N_p < \min\{L_{BR}, L_{RIS}\}$.

The transmitter employs the active transmit precoder $\boldsymbol{F}(t)$ to transmit the T data symbols $\boldsymbol{s}(t) \in \mathbb{C}^N$; and then, the receiver is combined with the corresponding receive beamformer $\mathbf{z}(t)$. Based on the above definitions, the signal $y(t)$ combined at the receiver can be written as

$$y(t) = \mathbf{z}^H(t) \boldsymbol{H} \boldsymbol{F}(t) \boldsymbol{s}(t) + n(t), \ \forall t = 1, \ldots, T, \tag{11}$$

where $\boldsymbol{H} \in \mathbb{C}^{M \times N}$ is the cascaded channel matrix that is given in (1). Here, $n(t)$ denotes the additive Gaussian noise. Without loss of generality, the pilot signal is set as $s(t) = 1$ during the training phase.

It is worth mentioning that the receiver often cannot directly observe $\boldsymbol{H}$. Instead, it observes a noisy version of $\mathbf{z}^H \boldsymbol{H} \boldsymbol{F}$, which causes a limitation to the application of the channel subspace sampling, especially when N and M are large for the channel matrix $\boldsymbol{H} \in \mathbb{C}^{M \times N}$, which makes channel estimation a challenging problem [47].

Fortunately, mmWave channels exhibit sparse scattering characteristics that can be utilized to substantially reduce the training overhead [48]. To facilitate channel estimation, we attempt to exploit the properties of Kronecker products and CS theory. Specifically, substituting (9) into (8), the received symbol is given by (12), shown at the bottom of the next page, where (a) is derived from

$$\begin{aligned} &\text{vec}(\boldsymbol{H}_{BRU}) \\ &= \text{vec}\left(\mathbf{A}_{BS} \boldsymbol{H}_\beta \mathbf{A}_{RIS,1}^H \boldsymbol{\Phi} \mathbf{A}_{RIS,2} \boldsymbol{H}_\delta \mathbf{A}_{UE}^H\right) \end{aligned}$$

$$
\begin{aligned}
&= \left(\mathbf{A}_{UE}^{*} \otimes \mathbf{A}_{BS}\right) \operatorname{vec}\left(\boldsymbol{H}_{\beta} \mathbf{A}_{RIS,1}^{H} \boldsymbol{\Phi} \mathbf{A}_{RIS,2} \boldsymbol{H}_{\delta}\right) \\
&= \left(\mathbf{A}_{UE}^{*} \otimes \mathbf{A}_{BS}\right) \left(\boldsymbol{H}_{\delta}^{T} \otimes \boldsymbol{H}_{\beta}\right) \operatorname{vec}\left(\mathbf{A}_{RIS,1}^{H} \boldsymbol{\Phi} \mathbf{A}_{RIS,2}\right) \\
&= \left(\mathbf{A}_{UE}^{*} \otimes \mathbf{A}_{BS}\right) \left(\operatorname{vec}\left(\mathbf{A}_{RIS,1}^{H} \boldsymbol{\Phi} \mathbf{A}_{RIS,2}\right)^{T} \otimes \boldsymbol{I}\right) \operatorname{vec}\left(\boldsymbol{H}_{\delta}^{T} \otimes \boldsymbol{H}_{\beta}\right) \\
&= \left(\mathbf{A}_{UE}^{*} \otimes \mathbf{A}_{BS}\right) \left(\mathbf{A}_{RIS,2}^{T} \otimes \mathbf{A}_{RIS,1}^{H}\right)^{T} \boldsymbol{h}_{BRU}, \qquad (13)
\end{aligned}
$$

Here, $(\cdot)^*$ represents the complex conjugate operator, $\boldsymbol{h}_{BU} \triangleq \operatorname{vec}(\boldsymbol{H}_{\alpha})$ and $\boldsymbol{h}_{BRU} \triangleq \left(\operatorname{vec}(\boldsymbol{\Phi})^{T} \otimes \boldsymbol{I}\right) \operatorname{vec}\left(\boldsymbol{H}_{\delta}^{T} \otimes \boldsymbol{H}_{\beta}\right)$, where $\otimes$ denotes the Kronecker product.

By collecting all measurements $y(t)$, the corresponding signal are stacked into a vector form $\mathbf{y} \triangleq [y(1), \ldots, y(T)]^{T}$. Then, we can obtain the expression in (14), as shown at the bottom of the next page, where

$$
\boldsymbol{\Psi}_{BU} = \begin{bmatrix} \boldsymbol{F}^{T}(1) \otimes \mathbf{z}^{H}(1) \\ \vdots \\ \boldsymbol{F}^{T}(T) \otimes \mathbf{z}^{H}(T) \end{bmatrix} \left(\mathbf{A}_{BU,2}^{*} \otimes \mathbf{A}_{BU,1}\right) \qquad (15)
$$

and

$$
\begin{aligned}
\boldsymbol{\Psi}_{BRU} = &\begin{bmatrix} \boldsymbol{F}^{T}(1) \otimes \mathbf{z}^{H}(1) \\ \vdots \\ \boldsymbol{F}^{T}(T) \otimes \mathbf{z}^{H}(T) \end{bmatrix} \left(\mathbf{A}_{UE}^{*} \otimes \mathbf{A}_{BS}\right) \\
&\times \left(\mathbf{A}_{RIS,2}^{T} \otimes \mathbf{A}_{RIS,1}^{H}\right)^{T}. \qquad (16)
\end{aligned}
$$

Since $\boldsymbol{h}_{BU}$ and $\boldsymbol{h}_{BRU}$ are sparse, the channel estimation problem based on (14) becomes a sparse recovery problem. The CS-based sparse signal recovery method has the potential to achieve a substantial training overhead reduction [34]. It follows that a high-dimensional sparse channel can be estimated by using the CS sparse recovery algorithm.

III. Parallel RIS-Assisted Channel Estimation

In this section, we will address the parallel channel estimation of RIS-assisted systems. In the proposed RIS-assisted mmWave system, the whole RIS-assisted channel is decomposed into a direct and the reflected channels. We can adjust the reflecting elements of the RIS to change the channel propagation environment. As illustrated in Fig. 1, the direct channel denotes the straight line channel from the BS to the user, while the reflected channel means that the incident signal is reflected by the RIS from the BS to the user.

A. Proposed RIS-Assisted Channel Estimation Framework

In this subsection, we will introduce the sparse representation framework of RIS-assisted channel estimation in detail. Based on (14), we aim to estimate the direct and reflected channels, simultaneously. As in the aforementioned observation, different regularizes lead to different properties of the representation of the channel coefficients. Therefore, it is unreasonable to assign equivalent regularization terms to the direct and the reflecting channels. To mitigate this issues, two regularization terms are developed to improve the performance of channel estimation. For the direct channel, there is a strong direct channel between the BS and the user. One way to enforce the sparsity of the solution is to use the reweighted ℓ_1-norm penalty term $\mathbf{g}_{BU}(\boldsymbol{h}_{BU})$. The reflecting channel suffers from a longer range than the direct channel, and the longer the distance, the greater the path loss. Therefore, the reflecting channel is much weaker than the direct channel. To capture weakly reflecting channels, the robust $\ell_{1,\tau}$ regularization term $\mathbf{g}_{BRU}(\boldsymbol{h}_{BRU})$ is proposed to achieve a better performance. To be more specific, the optimization problem can be formulated as

$$
\min_{\boldsymbol{h}, \boldsymbol{h}_{BU}, \boldsymbol{h}_{BRU}} \frac{1}{2} \|\mathbf{y} - \boldsymbol{\Psi} \boldsymbol{h}\|_2^2 + \mu_{BU} \mathbf{g}_{BU}(\boldsymbol{h}_{BU}) + \mu_{BRU} \mathbf{g}_{BRU}(\boldsymbol{h}_{BRU}), \qquad (17)
$$

where $\boldsymbol{\Psi} = \left[\boldsymbol{\Psi}_{BU}\ \boldsymbol{\Psi}_{BRU}\right]$ and $\boldsymbol{h} = \left[\boldsymbol{h}_{BU}^{T}\ \boldsymbol{h}_{BRU}^{T}\right]^{T}$, μ_{BU} and μ_{BRU} denote the regularization parameters, respectively. It is difficult to solve the nonconvex optimization problem (17), due to the multiple variables and the coupling between them.

To solve the optimization problem (17), the received signal $\mathbf{y}$ is divided into $\mathbf{y}_{BU}$ and $\mathbf{y}_{BRU}$ by exploiting the linearity of the direct and the reflected channels, respectively. Thus, we introduce the auxiliary variable $\boldsymbol{u}$ to reformulate the optimization problem (17) as

$$
\begin{aligned}
\min_{\boldsymbol{h}, \boldsymbol{h}_{BU}, \boldsymbol{h}_{BRU}} &\frac{1}{2} \|\mathbf{y} - \boldsymbol{\Psi}_{BU} \boldsymbol{h}_{BU} - \boldsymbol{\Psi}_{BRU} \boldsymbol{h}_{BRU}\|_2^2 + \mu_{BU} \mathbf{g}_{BU}(\boldsymbol{h}_{BU}) \\
&+ \mu_{BRU} \mathbf{g}_{BRU}(\boldsymbol{h}_{BRU}) + \frac{\kappa}{2} \|\boldsymbol{h} - \boldsymbol{u}\|_2^2 \\
s.t. \quad &\boldsymbol{u} = \boldsymbol{h}_{BU} + \boldsymbol{h}_{BRU}. \qquad (18)
\end{aligned}
$$

It follows that the optimization problem (18) includes three variables, which can be solved by the alternative optimization scheme. Then, we introduce the gradient descent-based alternating direction iterative framework to determine the direct and the reflected channels, respectively.

B. Direct Channel Estimation

In this subsection, the direct channel is estimated by exploiting the weighted ℓ_1-norm regularization model. It is due to the fact that a properly reweighted ℓ_1 norm approximates the ℓ_0-pseudo-norm, which actually needs to be minimized. It yields better results than the standard ℓ_1 norm. To this end, the direct channel $\boldsymbol{h}_{BU}$ is optimized by fitting the $\boldsymbol{h}_{BRU}$ as follows

$$
\min_{\boldsymbol{h}_{BU}} \frac{1}{2} \|\mathbf{y}_{BU} - \boldsymbol{\Psi}_{BU} \boldsymbol{h}_{BU}\|_2^2 + \mu_{BU} \mathbf{g}_{BU}(\boldsymbol{h}_{BU}), \qquad (19)
$$

$$
\begin{aligned}
y(t) &= \left(\boldsymbol{F}^{T}(t) \otimes \mathbf{z}^{H}(t)\right) \operatorname{vec}(\boldsymbol{H}) + n(t) \\
&\overset{(a)}{=} \left(\boldsymbol{F}^{T}(t) \otimes \mathbf{z}^{H}(t)\right) \left(\mathbf{A}_{UE}^{*} \otimes \mathbf{A}_{BS}\right) \boldsymbol{h}_{BU} + \left(\boldsymbol{F}^{T}(t) \otimes \mathbf{z}^{H}(t)\right) \operatorname{vec}\left(\boldsymbol{H}_{BR} \boldsymbol{\Phi} \boldsymbol{H}_{RU}\right) + n(t) \qquad (12) \\
&= \left(\boldsymbol{F}^{T}(t) \otimes \mathbf{z}^{H}(t)\right) \left(\mathbf{A}_{UE}^{*} \otimes \mathbf{A}_{BS}\right) \boldsymbol{h}_{BU} + \left(\boldsymbol{F}^{T}(t) \otimes \mathbf{z}^{H}(t)\right) \left(\mathbf{A}_{UE}^{*} \otimes \mathbf{A}_{BS}\right) \left(\mathbf{A}_{RIS,2}^{T} \otimes \mathbf{A}_{RIS,1}^{H}\right)^{T} \boldsymbol{h}_{BRU} + n(t).
\end{aligned}
$$

where $\mathbf{y}_{BU} = \mathbf{y} - \mathbf{\Psi}_{BRU}\boldsymbol{h}_{BRU}$ and $\mu_{BU} > 0$ denotes a regularization parameter. For the direct channel between the transmitter and receiver, since minimizing the ℓ_1-norm is an relaxation for ideal ℓ_0-norm minimization, the direct channel with the standard ℓ_1-norm minimization is limited to reflect the desired CSI requirements [49]. Compared with the standard ℓ_1-norm regularization, the successful application of weight ℓ_1-norm regularization indicates the better direct channel estimation, sparsity enhancement, and robustness to noise. Therefore, we utilize a weighted ℓ_1-norm regularization to characterize the direct channel information, which can be expressed as

$$\mathbf{g}_{BU}(\boldsymbol{h}_{BU}) = \mu_{BU}\sum_{i=1}^{L_{BU}} w(i)|h_{BU}(i)|, \tag{20}$$

where $h_{BU}(i)$ is the i-th element of the channel $\boldsymbol{h}_{BU}$ and $w(i) = \frac{1}{|h_{BU}(i)|+\varepsilon}$ is the i-th element of the weight vector, where $\varepsilon > 0$ is a small constant, whose role is to prevent the denominator from reaching zero.

To exploit the weighted ℓ_1-norm regularization (20), the optimization problem (19) is rewritten as

$$\min_{\boldsymbol{h}_{BU}} \frac{1}{2}\|\mathbf{y}_{BU} - \mathbf{\Psi}_{BU}\boldsymbol{h}_{BU}\|_2^2 + \mu_{BU}\sum_{i=1}^{L_{BU}} w(i)|h_{BU}(i)|. \tag{21}$$

Solving the problem (21) directly will incur huge complexity. To address this issue, we construct a proximal regularization of the problem (21) with simple algebra operations, which leads to an iterative scheme as

$$\min_{\boldsymbol{h}_{BU}} \frac{1}{2t}\left\|\boldsymbol{h}_{BU}^{(k)} + t\mathbf{\Psi}^T\left(\mathbf{y}_{BU} - \mathbf{\Psi}_{BU}\boldsymbol{h}_{BU}^{(k)}\right) - \boldsymbol{h}_{BU}^{(k+1)}\right\|_2^2, \tag{22}$$

where t is the step-size. It is observed that the solution of problem (22) is close to the optimal solution of (21), accompanied by a substantial reduction in the complexity.

To improve iteration speed and estimation accuracy, the iterative shrinkage thresholding algorithm with soft thresholding is utilized to (22), which yields

$$\boldsymbol{h}_{BU}^{(k+1)} = \mathcal{S}\left(\boldsymbol{h}_{BU}^{(k)} + t\mathbf{\Psi}^T(\mathbf{y}_{BU} - \mathbf{\Psi}_{BU}\boldsymbol{h}_{BU}^{(k)})\right). \tag{23}$$

where the shrinkage operator $\mathcal{S}_{BU}(i)$ can be expressed as

$$\mathcal{S}_{BU}(i) = \text{sign}\left(\boldsymbol{h}_{BU}^{(k)}\right)\left||\boldsymbol{h}_{BU}| - \frac{\mu_{BU}}{t}w(i)\right|, \tag{24}$$

and $\frac{\mu_{BU}}{t}$ is the thresholding value that plays a role in controlling the stepsize of each iteration.

C. Reflected Channel Estimation

In this subsection, the effectiveness and robustness of the $\ell_{1,\tau}$ regularization term is developed to capture weakly reflecting channels by fitting the direct channel $\boldsymbol{h}_{BU}$. Then, the solution to the problem (18) with respect to $\boldsymbol{h}_{BRU}$ can be rewritten as

$$\min_{\boldsymbol{h}_{BRU}} \frac{1}{2}\|\mathbf{y}_{BRU} - \mathbf{\Psi}_{BRU}\boldsymbol{h}_{BRU}\|_2^2 + \mu_{BRU}\mathbf{g}_{BRU}(\boldsymbol{h}_{BRU}), \tag{25}$$

where $\mathbf{y}_{BRU} = \mathbf{y} - \mathbf{\Psi}_{BU}\boldsymbol{h}_{BU}$.

To achieve precise performance, a robust $\ell_{1,\tau}$-norm is utilized to estimate the reflected channel by adjusting the parameter τ. To elaborate this phenomenon, an example is provided in Fig. 3. It is observed that different τ may lead to different solutions. However, the parameter τ is difficult to adjust because the $\ell_{1,\tau}$-norm model is non-convex. Therefore, it is important to determine the optimal value of the parameter τ, and an adaptive parameter τ is considered in this paper. Based on this, the robust $\ell_{1,\tau}$ regularization function is utilized, which can be expressed as follows

$$\mathbf{g}_{BRU}(\boldsymbol{h}_{BRU}) = \frac{1}{\tau}\sum_{i=1}^{L_{BR}} \log\left(\cosh\left(\tau\boldsymbol{h}_{BRU}(i)\right)\right). \tag{26}$$

It is evident that the $\ell_{1,\tau}$ regularization function in (26) is integrated into the problem (25), which may lead to the non-convex optimization problem. To address this issue, we utilize the first-order Taylor expansion to approximate $\mathbf{g}_{BRU}(\boldsymbol{h}_{BRU})$. Let $Q(\boldsymbol{h}_{BRU}) = \log\left(\cosh\left(\tau\boldsymbol{h}_{BRU}\right)\right)$, which can be given by

$$Q(\boldsymbol{h}_{BRU}) = Q(\boldsymbol{h}_{BRU}^{(k)}) + \left\langle \nabla Q(\boldsymbol{h}_{BRU}^{(k)}), \boldsymbol{h}_{BRU} - \boldsymbol{h}_{BRU}^{(k)}, \right\rangle, \tag{27}$$

where $Q(\boldsymbol{h}_{BRU}^{(k)})$ is the k-th iteration of the solution. By removing the constants, the derivative of (27) can be formulated as

$$Q'(\boldsymbol{h}_{BRU}) = \mu_{BRU}\left\langle \nabla \tanh(\tau\boldsymbol{h}_{BRU}^{(k)}), \boldsymbol{h}_{BRU}\right\rangle, \tag{28}$$

which may lead to the problem (25) as

$$\min_{\boldsymbol{h}_{BRU}} \frac{1}{2}\|\mathbf{y}_{BRU} - \mathbf{\Psi}_{BRU}\boldsymbol{h}_{BRU}\|_2^2 + \mu_{BRU}\left\langle \nabla \tanh(\tau\boldsymbol{h}_{BRU}^{(k)}), \boldsymbol{h}_{BRU}\right\rangle, \tag{29}$$

By utilizing the Karush-Kuhn-Tucher (KKT) condition, the solution of the problem (29) can be given by

$$\boldsymbol{h}_{BRU}^{(k+1)} = (\mathbf{\Psi}_{BRU}^H\mathbf{\Psi}_{BRU})^{-1}\left(\mathbf{\Psi}_{BRU}^H\mathbf{y}^{(k)} + \mu_{BRU}\tanh(\tau\boldsymbol{h}_{BRU}^{(k)})\right). \tag{30}$$

It follows that the channels $\boldsymbol{h}_{BU}$ and $\boldsymbol{h}_{BRU}$ can be optimized by alternating the solutions to the above two subproblems (19) and (25).

$$\begin{aligned}\mathbf{y} &= \begin{bmatrix}\boldsymbol{F}^T(1)\otimes\mathbf{z}^H(1)\\ \vdots \\ \boldsymbol{F}^T(T)\otimes\mathbf{z}^H(T)\end{bmatrix}\left(\mathbf{A}_{BU,1}^*\otimes\mathbf{A}_{BU,2}\right)\boldsymbol{h}_{BU} + \begin{bmatrix}\boldsymbol{F}^T(1)\otimes\mathbf{z}^H(1)\\ \vdots \\ \boldsymbol{F}^T(T)\otimes\mathbf{z}^H(T)\end{bmatrix}\left(\mathbf{A}_{UE}^*\otimes\mathbf{A}_{BS}\right)\left(\mathbf{A}_{RIS,2}^T\otimes\mathbf{A}_{RIS,1}^H\right)^T\boldsymbol{h}_{BRU} + \boldsymbol{n}\\ &= \begin{bmatrix}\mathbf{\Psi}_{BU}\ \mathbf{\Psi}_{BRU}\end{bmatrix}\begin{bmatrix}\boldsymbol{h}_{BU}\\ \boldsymbol{h}_{BRU}\end{bmatrix} + \boldsymbol{n} = \mathbf{\Psi}\boldsymbol{h} + \boldsymbol{n}.\end{aligned} \tag{14}$$

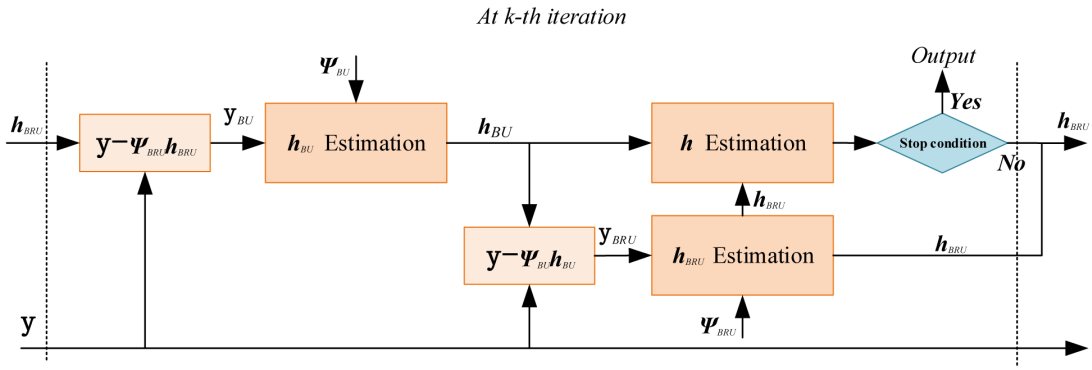

Fig. 2. The procedure of the proposed algorithm at the k-th iteration.

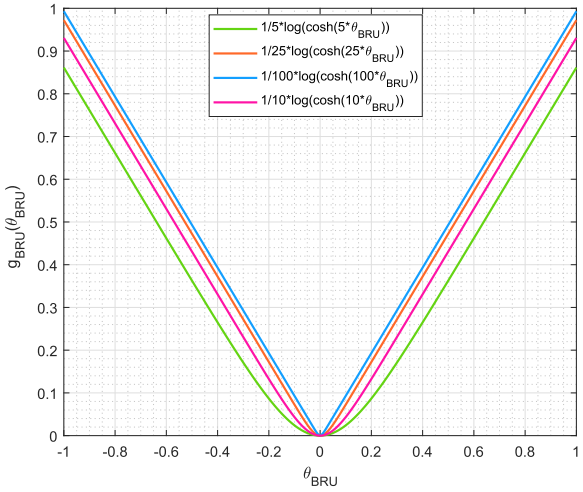

Fig. 3. The robust $\ell_{1,\tau}$-norm regularization function $\mathbf{g}_{BRU}(\boldsymbol{h}_{BRU}) = \frac{1}{\tau}\sum_{i=1}^{L}\log\left(\cosh\left(\tau h_{BRU}(i)\right)\right)$.

D. Parameter τ Updating

As we can see that the choosing of the parameter τ directly affects the ability of the regularization term. To reduce the artificial error, the parameter τ is updated in every iteration. The problem in (25) can be written as

$$\min_{\boldsymbol{h}_{BRU}} \frac{1}{2}\|\mathbf{y}_{BRU}-\boldsymbol{\Psi}_{BRU}\boldsymbol{h}_{BRU}\|_2^2 + \mu_{BRU}\log\left(\cosh\left(\tau\boldsymbol{h}_{BRU}\right)\right). \quad (31)$$

It is not difficult to observe that the optimization problem is a general convex constrained quadratic program whose optimal solution can be obtained by exploiting the KKT condition. That is

$$\tau^{(k)}\boldsymbol{h}_{BRU}^{(k)} = \operatorname{arctanh}\left(\frac{1}{\mu_{BRU}}\boldsymbol{\Psi}_{BRU}^{H}\left(\boldsymbol{\Psi}_{BRU}\boldsymbol{h}_{BRU}-\mathbf{y}_{BRU}^{(k)}\right)\right). \quad (32)$$

After taking the ℓ_2-norm at both sides of (32), the corresponding solution of the parameter $\tau^{(k)}$ can be rewritten as

$$\tau^{(k)} = \frac{\left\|\operatorname{arctanh}\left(\frac{1}{\mu_{BRU}}\boldsymbol{\Psi}_{BRU}^{H}(\boldsymbol{\Psi}_{BRU}\boldsymbol{h}_{BRU}-\mathbf{y}_{BRU}^{(k)})\right)\right\|_2}{\left\|\boldsymbol{h}_{BRU}^{(k)}\right\|_2+\eta}, \quad (33)$$

where a small constant $\eta > 0$ is provided to avoid the denominator from getting close to zero. It follows that the parameter τ can be updated in each iteration.

E. Hybrid Channel Updating

After the direct channel $\boldsymbol{h}_{BU}$ and the reflected channel $\boldsymbol{h}_{BRU}$ are estimated, the following optimization channel model is developed to characterize the hybrid channel, which can be formulated as

$$\min_{\boldsymbol{h}}\frac{1}{2}\|\mathbf{y}-\boldsymbol{\Psi}\boldsymbol{h}\|_2^2+\frac{\kappa}{2}\|\boldsymbol{h}-\boldsymbol{u}\|_2^2. \quad (34)$$

It is obvious that the optimization problem (34) is a convex problem. By utilizing the Karush-Kuhn-Tucher (KKT) condition, we have

$$\boldsymbol{h} = \left(\boldsymbol{\Psi}^H\boldsymbol{\Psi}+\kappa\boldsymbol{I}\right)^{-1}\left(\boldsymbol{\Psi}^H\mathbf{y}+\kappa\boldsymbol{u}\right). \quad (35)$$

Through above three-stage scheme, the channels $\boldsymbol{h}_{BU}$, $\boldsymbol{h}_{BRU}$ and $\boldsymbol{h}$ can be effectively decoupled and provide better results, which is illustrated in Algorithm 1. To ensure that the proposed Algorithm 1 can converge to a stable value, the stopping criterion $\|\boldsymbol{h}^{(k)}-\boldsymbol{h}^{(k-1)}\|_2^2 \le \varepsilon$ is considered for the end of Algorithm 1. When the error between the current iteration and the previous iteration is less than ε (e.g., $\varepsilon = 10^{-3}$), it implies that the proposed algorithm can converge to the neighborhood of the stable value. We also provide a diagram to explain the k-th iteration procedure of the proposed algorithm in Fig.2.

F. Complexity Analysis

It is shown in Algorithm 1 that the $\boldsymbol{h}_{BU}$, $\boldsymbol{h}_{BRU}$ and $\boldsymbol{h}$ are alternatingly optimized. We estimate the computational complexity of the proposed Algorithm 1 by computing the number of required multiplications. Assumption the number of iteration for the Algorithm 1 is I_{iter}. Under this assumption, the overall computational complexity of Algorithm 1 is caused by solving the problem (17), which consists of a series of subproblems, e.g., the direct channel estimation subproblem (19), the reflected channel estimation subproblem (25) and the hybrid channel estimation subproblem (34). For the direct channel estimation subproblem (19), the solution with respect to $\boldsymbol{h}_{BU}$, whose complexity is $\mathcal{O}(TL_{BR}L_{RU})$. For the reflected channel estimation subproblem (25), the parameter τ need to be calculated, which introduces the complexity of $\mathcal{O}((MN)^2T+MNT^2)$, and the complexity of estimating $\boldsymbol{h}_{BRU}$ is approximated as $\mathcal{O}((MN)^3+MNT+MNT^2)$. For the solution with respect to $\boldsymbol{h}$, $(\boldsymbol{\Psi}^H\boldsymbol{\Psi}+\kappa\boldsymbol{I})^{-1}$ and $\boldsymbol{\Psi}^H\mathbf{y}$ can be computed in advance and the complexity of estimating

Algorithm 1 Parallel Channel Estimation Algorithm

Input: Given the measurement $\mathbf{y}$, and the matrices $\boldsymbol{\Psi}_{BRU}$, $\boldsymbol{\Psi}_{BU}$
Initialization: $k = 0$, $\boldsymbol{h}^{(0)} = \mathbf{0}$;
repeat
  Update $\mathbf{y}_{BU}$ with $\mathbf{y}_{BU} = \mathbf{y} - \boldsymbol{\Psi}_{BRU}\boldsymbol{h}_{BRU}$;
  1. estimate $\boldsymbol{h}_{BU}$ by solving
    $\min_{\boldsymbol{h}_{BU}} \frac{1}{2}\|\mathbf{y}_{BU} - \boldsymbol{\Psi}_{BU}\boldsymbol{h}_{BU}\|_2^2 + \mu_{BU}\mathbf{g}_{BU}(\boldsymbol{h}_{BU})$;
  Update $\mathbf{y}_{BRU}$ with $\mathbf{y}_{BRU} = \mathbf{y} - \boldsymbol{\Psi}_{BU}\boldsymbol{h}_{BU}$;
  2. estimate $\boldsymbol{h}_{BRU}$ by solving
    $\min_{\boldsymbol{h}_{BRU}} \frac{1}{2}\|\mathbf{y}_{BRU} - \boldsymbol{\Psi}_{BRU}\boldsymbol{h}_{BRU}\|_2^2 + \mu_{BRU}\mathbf{g}_{BRU}(\boldsymbol{h}_{BRU})$;
  Update the parameter τ by solving (33);
  Update $\boldsymbol{u}$ with $\boldsymbol{u} = \boldsymbol{h}_{BU} + \boldsymbol{h}_{BRU}$;
  3. estimate $\boldsymbol{h}^{(k+1)}$ by solving
    $\min_{\boldsymbol{h}} \frac{1}{2}\|\mathbf{y} - \boldsymbol{\Psi}\boldsymbol{h}\|_2^2 + \frac{\kappa}{2}\|\boldsymbol{h} - \boldsymbol{u}\|_2^2$
until $\left\|\boldsymbol{h}^{(k+1)} - \boldsymbol{h}^{(k)}\right\|_2 \leq \varepsilon$
end
Output $\boldsymbol{h}_{BU}$, $\boldsymbol{h}_{BRU}$ $\boldsymbol{h}$.

$\mathcal{O}(TN_{\tau_1}N_{\tau_2}N_{\tau_1}N_{\tau_2})$. Based on the analysis above, the complexity of Algorithm 1 is expressed as $\mathcal{O}(I_{iter}(TL_{BR}L_{RU} + (MN)^3 + MNT^2 + TN_{\tau_1}N_{\tau_2}N_{\tau_1}N_{\tau_2}))$.

IV. Simulation Results

In this section, we carry out the simulations to illustrate the effectiveness of our proposed algorithm. The RIS is practically deployed with a planar antenna array to enhance the communication link. The system bandwidth and carrier frequency are set to 20 MHz and 2 GHz, respectively. The simulation parameters are set as $N_{UE} = 6$ and $N_t = 128$. Due to the limited pilot resources, we consider the reflecting elements $N_{RIS} = 16, 36, 64, 128$, respectively. To help prospective readers to see the different parameters, the parameter settings are listed in Table I. To quantify the estimator performance, the average normalized MSE between the estimated and the original channel are calculated through Monte Carlo simulations, which are averaged over the channel realizations. The corresponding normalized MSE is defined as

$$\text{NMSE} = \frac{\|\boldsymbol{h} - \hat{\boldsymbol{h}}\|_2^2}{\|\boldsymbol{h}\|_2^2}, \tag{36}$$

where $\boldsymbol{h}$ and $\hat{\boldsymbol{h}}$ are the original and the estimated channels, respectively. To verify the estimation performance, we also define the EVM as the performance metric that is calculated as

$$\text{EVM} = 10\log 10\left(\frac{\frac{1}{N}\sum_{k=1}^{N} e_k}{\frac{1}{N}\sum_{k=1}^{N}(I_k^2 + Q_k^2)}\right), \tag{37}$$

where e_k is the estimated error that can be expressed as $e_k = (I_k - \hat{I}_k)^2 + (Q_k - \hat{Q}_k)^2$. Here, I_k and Q_k denote the In-phase (I) component and the Quadrature phase (Q) component, respectively.

TABLE I
The Proposed Channel Framework Parameters for Simulation

Parameters	Value
System bandwidth	200 MHz
Reflecting elements	$N_{RIS} = 16, 36, 64, 128$
Carrier frequency	2 GHz
Number of antennas at BS	$N_t = 128$
Number of radio frequency	$N_{RF} = 6:2:24$
The antenna spacing	$d = \frac{\lambda_c}{2}$
Number of paths	$P = 5$
Signal-to-noise ratio (SNR)	$-20:5:25$

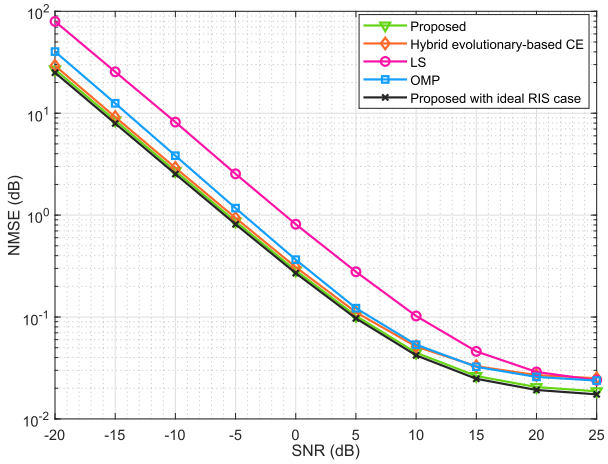

Fig. 4. NMSE performance of the proposed channel estimator versus the SNRs in dB.

A. Performance Comparison

The proposed channel estimator is compared with the conventional schemes, such as the LS, OMP [50] and hybrid evolutionary-based channel estimator [14]. As observed from Fig. 4, the simulation results show that the proposed estimator is consistent with the theoretical curves along with the increase of SNRs. Meanwhile, as the SNR level increases, the NMSEs for all those estimators decreases and gradually stabilizes. This favorable result can be attributed to the fact that when the SNR level is low, the effect of noise gives a dominant influence on the performance of channel estimation. It is acknowledged that the LS estimator is vulnerable to noise, this conclusion also is validated in our simulations that the LS estimator performs poorly in the low SNR zone. The main reason is that the LS estimation contains both scale-factor and bias errors. The scale-factor error is caused by the auto-correlation of the stochastic parametric uncertainties in the measurement matrix, and the bias error comes from the correlation between the uncertain stochastic parameters and measurement noises. That is to say, the proposed scheme is more robust than the LS estimator. Meanwhile, the OMP estimator reaches a similar performance as the LS estimator without prior knowledge of CSI. The simulation results show that whenever the SNR value is small or large, the proposed algorithm always achieves a performance improvement compared with the LS and the OMP estimators, which verifies that the proposed scheme can well be applied to the different SNR levels.

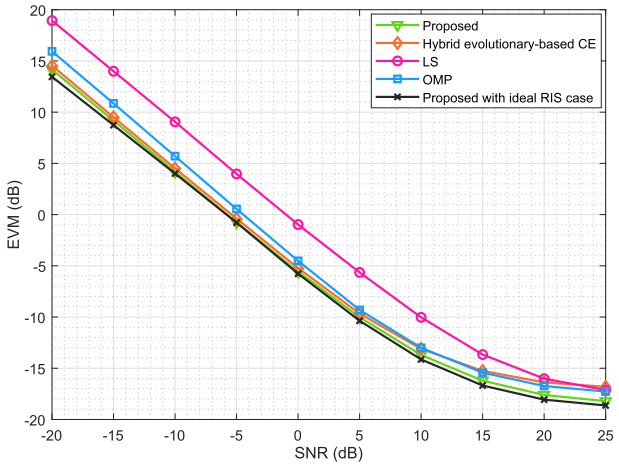

Fig. 5. EVM performance of the proposed channel estimator versus the SNRs in dB.

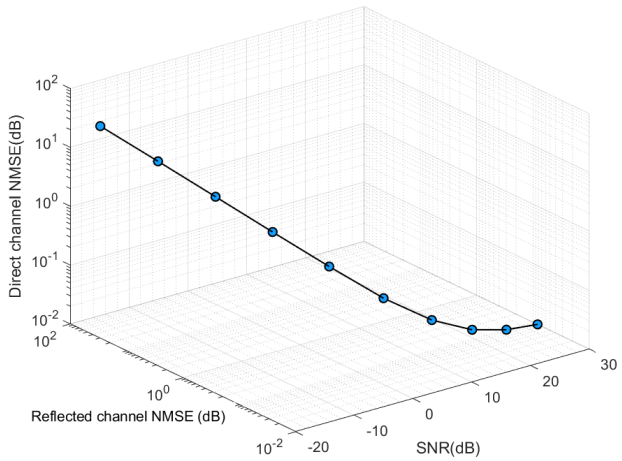

Fig. 6. NMSE performance comparisons between the direct and the reflected channel estimation.

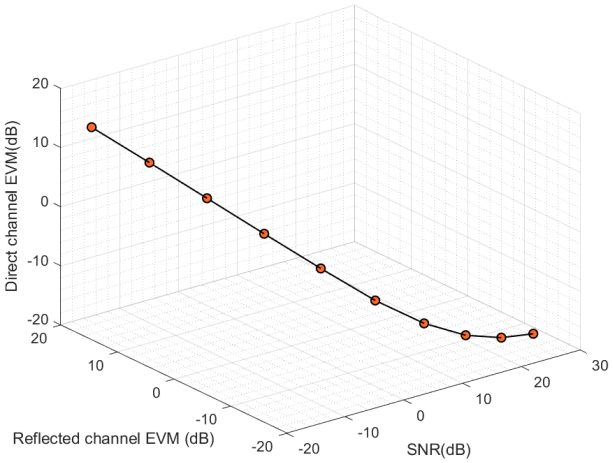

Fig. 7. EVM performance comparisons between the direct and the reflected channel estimation.

In addition, the hybrid evolutionary-based channel estimator also is employed for comparison. Simulation results confirm that a significant improvement is obtained by the proposed estimator under the RIS-assisted channel. It is important to point out that the effect of noise can be almost ignored in the high SNR zone, and hence it can be seen that the three estimators converge to a stable state, when the SNR levels are not lower than 20. More importantly, it can be observed that the curves "Ideal RISs case" and " non-ideal $\mathcal{F}_2$ case" are very close. The essential reason is that actually most of the RIS elements have an amplitude equal to 1. It implies that they are not need to design an amplitude-controllable RIS for wireless communications.

Next, we study of the EVM performance on the different SNR levels for the different estimators in Fig. 5. We can observe that as the SNR increases, the EVM performance of all estimators improve. Furthermore, as can be observed in Fig. 5 that the proposed scheme achieves a better performance in the entire SNR range, and the hybrid evolutionary-based channel estimator is close to the proposed scheme at low SNRs, while the hybrid evolutionary-based channel estimator suffers from a slight performance degradation at high SNRs. Another interesting observation is that the EVM performance of the LS reduces rapidly with the increase of SNRs, while for the OMP estimator, it reduces slowly. Moreover, the performance gap between the proposed estimator and the hybrid evolutionary-based channel estimator becomes larger as the SNR increases, which proves that the proposed channel estimator is available in RIS-assisted communication scenarios, especially in the higher SNR regime.

In Figs. 6 and 7, the simulated NMSE of the channel estimation approach for the direct and the reflected channels are depicted, where the SNR levels from -20 dB and 30 dB. As seen from Fig. 6, it is observed that the NMSEs of the direct and reflected channels decrease significantly with the SNR levels increasing. Moreover, we observe a similar behavior in Fig. 7. The EVMs of the direct and the reflected channels are differences as the SNR increases. This is because the proposed scheme utilizes the weighted ℓ_1-norm and robust $\ell_{1,\tau}$-norm to improve the estimation accuracy. From these results, we observe that the direct and the reflected channels both offer a promising performance in terms of NMSEs and EVMs. This will attract a great attention in the application of the RIS to the existing IoT systems to boost the channel estimation process.

Finally, the pilot contamination problem is investigated to verify the robustness of the proposed estimator for different pilot lengths and radio frequency (RF) chains. All simulation results are depicted in Fig. 8. It is obvious that there exists an increasing NMSE performance loss when the number of the pilots is reduced. Similar results are also demonstrated in Fig. 9 as the EVM performance of all estimators exhibit similar results as the NMSE performance. These results verify the effectiveness of the proposed estimator. However, as depicted in Fig. 8 and 9, the performance of the proposed channel estimator is almost unaffected by the high SNR levels. This is because the effect of the noise can be almost ignored in the high SNR zone, and hence our findings show that the proposed estimator has the best performance in terms of NMSE and EVM values.

B. Extension to the Impact of the Number of RIS Elements

As a further experiment, we investigate the impact of the number of RIS elements on the achievable rate. Fig. 10 shows the impact of the number of RIS elements between the BS

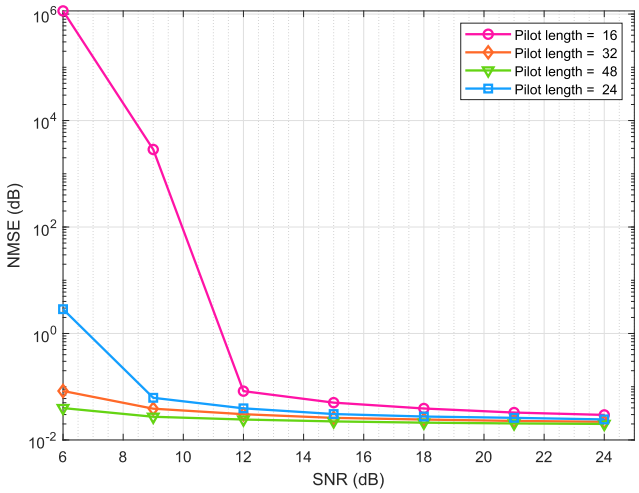

Fig. 8. NMSE performance of the proposed channel estimator versus the number of RF chains.

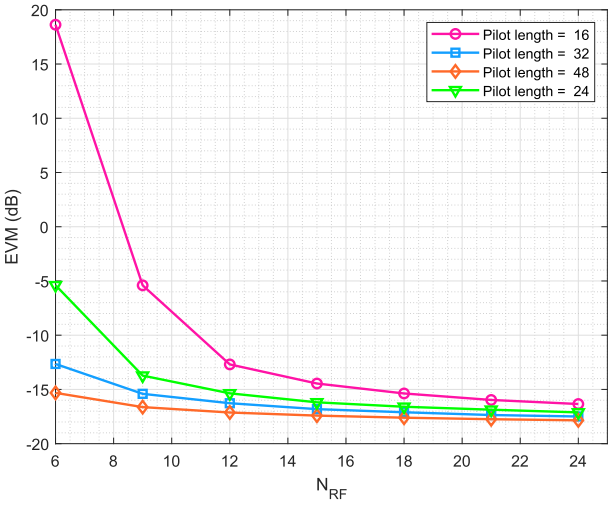

Fig. 9. EVM performance of the proposed channel estimator versus the number of RF chains.

and the RIS on the achievable rate performance. It can be seen that the performance of the proposed algorithm degrades when the number of RIS elements increases under the given pilot overhead, due to the fact that the number of parameters (sparsity level) to be estimated increases. This finding is also in agreement with similar observations found in the achievable rate studied in the previous section, which verifies the superiority of the proposed system model and design once again.

C. Convergence Analysis

In this subsection, the convergence behavior of the parallel channel estimation algorithm is evaluated by illustrating how the number of iterations affect the NMSE performance behavior. It can be seen in Fig. 11 that the proposed algorithm can converge to a stable value, and the different SNR levels affect the convergence result of the algorithm. In particular, the NMSE value gradually decreases and converges to a fixed value after approximately 13 iterations. This result demonstrates that the proposed algorithm has the ability to converge to a stable point.

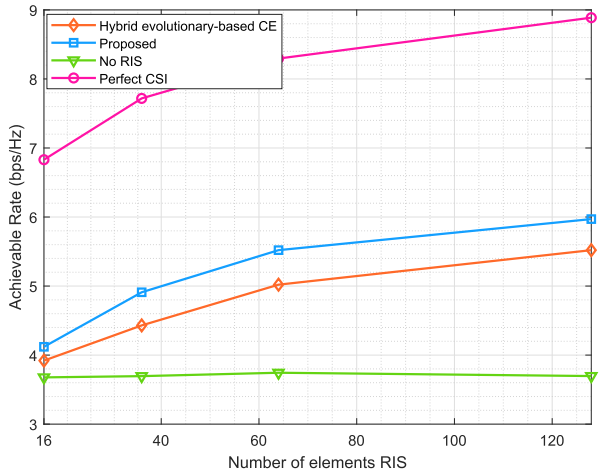

Fig. 10. Achievable rate versus the number of RIS elements performance.

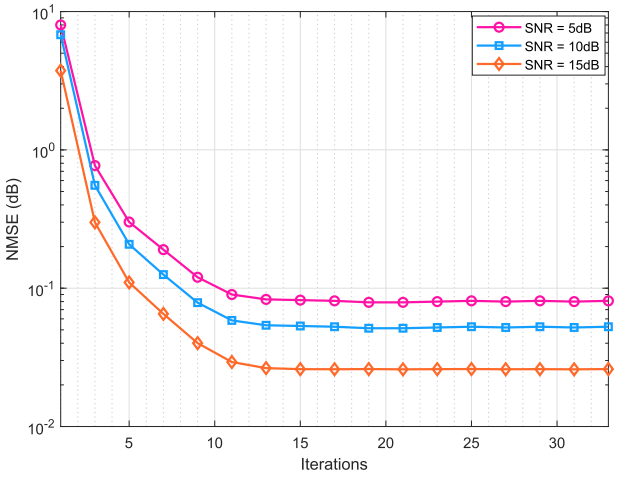

Fig. 11. NMSE performance of the proposed channel estimator versus the number of iteration.

V. Conclusion

In this paper, we investigate the problem of parallel channel estimation for RIS-assisted IoT systems using merely a small number of the pilot symbols. Under the proposed framework, the weighted ℓ_1-norm minimization and the robust $\ell_{1,\tau}$-norm minimization criterion are utilized to efficiently perform the direct and the reflected channel estimation, respectively. Then, we reformulate the channel estimation problem as a sparse recovery problem and utilize the gradient descent-based alternating direction algorithm to obtain a feasible solution with a few pilot symbols. Simulation results confirm the desirable performance of the proposed scheme compared to the LS, the OMP and the hybrid evolutionary-based estimator, as all of them work for RIS-assisted communication scenarios. Moreover, it is interesting to observe that the number of RIS unit elements and RF chains have a significant effect on the performance of the proposed estimator.

References

[1] J. Wang, G. Wang, B. Li, H. Yang, Y. Hu, and A. Schmeink, "Massive MIMO two-way relaying systems with SWIPT in IoT networks," *IEEE Internet Things J.*, vol. 8, no. 20, pp. 15126–15139, Oct. 2021.

[2] T. Jiang, Y. Shi, J. Zhang, and K. B. Letaief, "Joint activity detection and channel estimation for IoT networks: Phase transition and computation-estimation tradeoff," *IEEE Internet Things J.*, vol. 6, no. 4, pp. 6212–6225, Aug. 2019.

[3] S. Fang, G. Chen, Z. Abdullah, and Y. Li, "Intelligent omni surface-assisted secure MIMO communication networks with artificial noise," *IEEE Commun. Lett.*, vol. 26, no. 6, pp. 1231–1235, Jun. 2022.

[4] Z. Chen, J. Tang, N. Zhao, M. Liu, and D. K. C. So, "Hybrid beamforming with discrete phase shifts for RIS-assisted multiuser SWIPT system," *IEEE Wireless Commun. Lett.*, vol. 12, no. 1, pp. 104–108, Jan. 2023.

[5] S. Sun and H. Yan, "Channel estimation for reconfigurable intelligent surface-assisted wireless communications considering Doppler effect," *IEEE Wireless Commun. Lett.*, vol. 10, no. 4, pp. 790–794, Apr. 2021.

[6] Q. Cheng et al., "Reconfigurable intelligent surfaces: Simplified-architecture transmitters—From theory to implementations," *Proc. IEEE*, vol. 110, no. 9, pp. 1266–1289, Sep. 2022.

[7] K. Zhi, C. Pan, H. Ren, and K. Wang, "Ergodic rate analysis of reconfigurable intelligent surface-aided massive MIMO systems with ZF detectors," *IEEE Commun. Lett.*, vol. 26, no. 2, pp. 264–268, Feb. 2022.

[8] H. Niu, Z. Chu, F. Zhou, and Z. Zhu, "Simultaneous transmission and reflection reconfigurable intelligent surface assisted secrecy MISO networks," *IEEE Commun. Lett.*, vol. 25, no. 11, pp. 3498–3502, Nov. 2021.

[9] Q. Wu, W. Chen, M. Tao, J. Li, H. Tang, and J. Wu, "Resource allocation for joint transmitter and receiver energy efficiency maximization in downlink OFDMA systems," *IEEE Trans. Commun.*, vol. 63, no. 2, pp. 416–430, Feb. 2015.

[10] P. Chen, Z. Chen, B. Zheng, and X. Wang, "Efficient DOA estimation method for reconfigurable intelligent surfaces aided UAV swarm," *IEEE Trans. Signal Process.*, vol. 70, pp. 743–755, 2022.

[11] C. Huang, G. C. Alexandropoulos, C. Yuen, and M. Debbah, "Indoor signal focusing with deep learning designed reconfigurable intelligent surfaces," in *Proc. IEEE 20th Int. Workshop Signal Process. Adv. Wireless Commun. (SPAWC)*, Jul. 2019, pp. 1–5.

[12] S. Ma, W. Shen, J. An, and L. Hanzo, "Wideband channel estimation for IRS-aided systems in the face of beam squint," *IEEE Trans. Wireless Commun.*, vol. 20, no. 10, pp. 6240–6253, Oct. 2021.

[13] A. M. Elbir and S. Coleri, "Federated learning for channel estimation in conventional and RIS-assisted massive MIMO," 2020, *arXiv:2008.10846*.

[14] Z. Chen, J. Tang, X. Y. Zhang, D. K. C. So, S. Jin, and K.-K. Wong, "Hybrid evolutionary-based sparse channel estimation for IRS-assisted mmWave MIMO systems," *IEEE Trans. Wireless Commun.*, vol. 21, no. 3, pp. 1586–1601, Mar. 2022.

[15] Y. Gao, J. Xu, W. Xu, D. W. K. Ng, and M.-S. Alouini, "Distributed IRS with statistical passive beamforming for MISO communications," *IEEE Wireless Commun. Lett.*, vol. 10, no. 2, pp. 221–225, Feb. 2021.

[16] J. Mirza and B. Ali, "Channel estimation method and phase shift design for reconfigurable intelligent surface assisted MIMO networks," *IEEE Trans. Cogn. Commun. Netw.*, vol. 7, no. 2, pp. 441–451, Jun. 2021.

[17] W. Yang, H. Li, M. Li, Y. Liu, and Q. Liu, "Channel estimation for practical IRS-assisted OFDM systems," in *Proc. IEEE Wireless Commun. Netw. Conf. Workshops (WCNCW)*, Mar. 2021, pp. 1–6.

[18] X. Hu, R. Zhang, and C. Zhong, "Semi-passive elements assisted channel estimation for intelligent reflecting surface-aided communications," *IEEE Trans. Wireless Commun.*, vol. 21, no. 2, pp. 1132–1142, Feb. 2022.

[19] Z. Wang, L. Liu, and S. Cui, "Channel estimation for intelligent reflecting surface assisted multiuser communications: Framework, algorithms, and analysis," *IEEE Trans. Wireless Commun.*, vol. 19, no. 10, pp. 6607–6620, Oct. 2020.

[20] Y. Jin, J. Zhang, X. Zhang, H. Xiao, B. Ai, and D. W. K. Ng, "Channel estimation for semi-passive reconfigurable intelligent surfaces with enhanced deep residual networks," *IEEE Trans. Veh. Technol.*, vol. 70, no. 10, pp. 11083–11088, Oct. 2021.

[21] D. Mishra and H. Johansson, "Channel estimation and low-complexity beamforming design for passive intelligent surface assisted MISO wireless energy transfer," in *Proc. IEEE Int. Conf. Acoust., Speech Signal Process. (ICASSP)*, May 2019, pp. 4659–4663.

[22] N. Suga and T. Furukawa, "Scalar ambiguity estimation based on maximum likelihood criteria for totally blind channel estimation in block transmission systems," *IEEE Trans. Wireless Commun.*, vol. 20, no. 4, pp. 2608–2620, Apr. 2021.

[23] J. He, H. Wymeersch, and M. Juntti, "Channel estimation for RIS-aided mmWave MIMO systems via atomic norm minimization," *IEEE Trans. Wireless Commun.*, vol. 20, no. 9, pp. 5786–5797, Sep. 2021.

[24] T. L. Jensen and E. De Carvalho, "An optimal channel estimation scheme for intelligent reflecting surfaces based on a minimum variance unbiased estimator," in *Proc. IEEE Int. Conf. Acoust., Speech Signal Process. (ICASSP)*, May 2020, pp. 5000–5004.

[25] J. An, C. Xu, L. Gan, and L. Hanzo, "Low-complexity channel estimation and passive beamforming for RIS-assisted MIMO systems relying on discrete phase shifts," *IEEE Trans. Commun.*, vol. 70, no. 2, pp. 1245–1260, Feb. 2022.

[26] J. An et al., "Codebook-based solutions for reconfigurable intelligent surfaces and their open challenges," *IEEE Wireless Commun.*, early access, doi: 10.1109/MWC.010.2200312.

[27] C. Xu et al., "Channel estimation for reconfigurable intelligent surface assisted high-mobility wireless systems," *IEEE Trans. Veh. Technol.*, vol. 72, no. 1, pp. 718–734, Jan. 2023.

[28] Z. Chen, J. Ye, and L. Huang, "A two-stage beamforming design for active RIS aided dual functional radar and communication," in *Proc. IEEE Wireless Commun. Netw. Conf. (WCNC)*, Mar. 2023, pp. 1–6.

[29] M. Luan, B. Wang, Z. Chang, T. Hämäläinen, and F. Hu, "Robust beamforming design for RIS-aided integrated sensing and communication system," *IEEE Trans. Intell. Transp. Syst.*, vol. 24, no. 6, pp. 6227–6243, Jun. 2023.

[30] P. Wang, J. Fang, H. Duan, and H. Li, "Compressed channel estimation for intelligent reflecting surface-assisted millimeter wave systems," *IEEE Signal Process. Lett.*, vol. 27, pp. 905–909, 2020.

[31] M. Ke, Z. Gao, Y. Wu, X. Gao, and R. Schober, "Compressive sensing-based adaptive active user detection and channel estimation: Massive access meets massive MIMO," *IEEE Trans. Signal Process.*, vol. 68, pp. 764–779, 2020.

[32] F. Gómez-Cuba and A. J. Goldsmith, "Compressed sensing channel estimation for OFDM with non-Gaussian multipath gains," *IEEE Trans. Wireless Commun.*, vol. 19, no. 1, pp. 47–61, Jan. 2020.

[33] A. Taha, M. Alrabeiah, and A. Alkhateeb, "Enabling large intelligent surfaces with compressive sensing and deep learning," *IEEE Access*, vol. 9, pp. 44304–44321, 2021.

[34] Z. Chen, J. Tang, H. Tang, X. Zhang, D. K. C. So, and K.-K. Wong, "Channel estimation of IRS-aided communication systems with hybrid multiobjective optimization," in *Proc. IEEE Int. Conf. Commun.*, Jun. 2021, pp. 1–6.

[35] T. Jiang, H. V. Cheng, and W. Yu, "Learning to beamform for intelligent reflecting surface with implicit channel estimate," in *Proc. GLOBECOM IEEE Global Commun. Conf.*, Dec. 2020, pp. 1–6.

[36] N. K. Kundu and M. R. McKay, "Channel estimation for reconfigurable intelligent surface aided MISO communications: From LMMSE to deep learning solutions," *IEEE Open J. Commun. Soc.*, vol. 2, pp. 471–487, 2021.

[37] S. Liu, Z. Gao, J. Zhang, M. D. Renzo, and M. Alouini, "Deep denoising neural network assisted compressive channel estimation for mmWave intelligent reflecting surfaces," *IEEE Trans. Veh. Technol.*, vol. 69, no. 8, pp. 9223–9228, Aug. 2020.

[38] Z. Chen et al., "Offset learning based channel estimation for intelligent reflecting surface-assisted indoor communication," *IEEE J. Sel. Topics Signal Process.*, vol. 16, no. 1, pp. 41–55, Jan. 2022.

[39] C. Liu, X. Liu, D. W. K. Ng, and J. Yuan, "Deep residual learning for channel estimation in intelligent reflecting surface-assisted multi-user communications," *IEEE Trans. Wireless Commun.*, vol. 21, no. 2, pp. 898–912, Feb. 2022.

[40] X. Yu, V. Jamali, D. Xu, D. W. K. Ng, and R. Schober, "Smart and reconfigurable wireless communications: From IRS modeling to algorithm design," *IEEE Wireless Commun.*, vol. 28, no. 6, pp. 118–125, Dec. 2021.

[41] Z. Zhang and L. Dai, "A joint precoding framework for wideband reconfigurable intelligent surface-aided cell-free network," *IEEE Trans. Signal Process.*, vol. 69, pp. 4085–4101, 2021.

[42] X. Li, J. Fang, H. Li, and P. Wang, "Millimeter wave channel estimation via exploiting joint sparse and low-rank structures," *IEEE Trans. Wireless Commun.*, vol. 17, no. 2, pp. 1123–1133, Feb. 2018.

[43] A. Alkhateeb, O. E. Ayach, G. Leus, and R. W. Heath, "Channel estimation and hybrid precoding for millimeter wave cellular systems," *IEEE J. Sel. Topics Signal Process.*, vol. 8, no. 5, pp. 831–846, Oct. 2014.

[44] J. Wang, L. Kong, and M.-Y. Wu, "Capacity of wireless ad hoc networks using practical directional antennas," in *Proc. IEEE Wireless Commun. Netw. Conf.*, Apr. 2010, pp. 1–6.

[45] J. Zhang, H. Du, Q. Sun, B. Ai, and D. W. K. Ng, "Physical layer security enhancement with reconfigurable intelligent surface-aided networks," *IEEE Trans. Inf. Forensics Security*, vol. 16, pp. 3480–3495, 2021.

[46] W. Tang et al., "Wireless communications with reconfigurable intelligent surface: Path loss modeling and experimental measurement," *IEEE Trans. Wireless Commun.*, vol. 20, no. 1, pp. 421–439, Jan. 2021.

[47] S. Hur, T. Kim, D. J. Love, J. V. Krogmeier, T. A. Thomas, and A. Ghosh, "Millimeter wave beamforming for wireless backhaul and access in small cell networks," *IEEE Trans. Commun.*, vol. 61, no. 10, pp. 4391–4403, Oct. 2013.

[48] M. R. Akdeniz et al., "Millimeter wave channel modeling and cellular capacity evaluation," *IEEE J. Sel. Areas Commun.*, vol. 32, no. 6, pp. 1164–1179, Jun. 2014.

[49] X. Huang, Y. Liu, L. Shi, S. Van Huffel, and J. A. K. Suykens, "Two-level $\ell 1$ minimization for compressed sensing," *Signal Process.*, vol. 108, pp. 459–475, Mar. 2015.

[50] Y. Liu, S. Zhang, F. Gao, J. Tang, and O. A. Dobre, "Cascaded channel estimation for RIS assisted mmWave MIMO transmissions," *IEEE Wireless Commun. Lett.*, vol. 10, no. 9, pp. 2065–2069, Sep. 2021.

Zhen Chen (Senior Member, IEEE) received the M.S. degree in software engineering from Xiamen University in 2012 and the Ph.D. degree in electronic engineering from the South China University of Technology (SCUT), Guangzhou, China, in 2019.

From 2020 to 2023, he was a Research Fellow with the Hong Kong Applied Science and Technology Research Institute, Hong Kong. He is currently an Associate Professor with the School of Electronic and Information Engineering, SCUT. His current research interests include array signal processing, Integrated radar and communication, channel estimation, UAV communications and 5G/6G networks. He has served as Technical Program Committee (TPC) Co-chair/member and Session Chair for a number of conferences. He was the Exemplary Reviewer of several IEEE journals. He was a co-recipient of EAI AICON 2021, ICICSP 2022, ICCC 2023 and ICICSP 2023 Best Paper Awards.

Lei Huang (Senior Member, IEEE) was born in Guangdong, China. He received the B.Sc., M.Sc., and Ph.D. degrees in electronic engineering from Xidian University, Xi'an, China, in 2000, 2003, and 2005, respectively. From 2005 to 2006, he was a Research Associate with the Department of Electrical and Computer Engineering, Duke University, Durham, NC, USA. From 2009 to 2010, he was a Research Fellow with the Department of Electronic Engineering, City University of Hong Kong, and a Research Associate with the Department of Electronic Engineering, The Chinese University of Hong Kong. From 2012 to 2014, he was a Professor with the Department of Electronic and Information Engineering, Harbin Institute of Technology Shenzhen Graduate School. Since 2014, he has been with the College of Electronics and Information Engineering, Shenzhen University, Shenzhen, China, where he is currently a Distinguished Professor and the Vice Dean. His research interests include spectral estimation, array signal processing, and statistical signal processing.

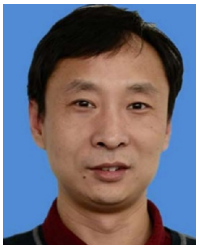

Shuqiang Xia received the master's degree in signal and information processing from the Nanjing University of Science and Technology, China, in 2002. He is currently a Senior Communication Research Expert with ZTE Corporation. His research interests include integrated sensing and communications (ISAC), carrier aggregation (CA), and ultra-reliable low-latency communications (URLLC). He was a recipient of the China Patent Gold Award and Second Prize of National Technological Invention Award.

Boyi Tang (Student Member, IEEE) received the B.Eng. degree in communication engineering from the University of Electronic Science and Technology of China and the B.Eng. degree (Hons.) in electronics and electrical engineering from the University of Glasgow in 2022. She is currently pursuing the Ph.D. degree with the Department of Electronic and Electrical Engineering, University College London, U.K. Her research interests include fluid antenna, physical layer security, and mathematical optimization.

Martin Haardt (Fellow, IEEE) received the Diplom-Ingenieur (M.S.) degree in electrical engineering from Ruhr-University Bochum, Germany, in 1991, and the Doktor-Ingenieur (Ph.D.) degree from the Munich University of Technology, Germany, in 1996.

During his diploma studies he also studied as a Visiting Scholar with Purdue University, USA. Since 2001, he has been a Full Professor with the Department of Electrical Engineering and Information Technology and the Head of the Communications Research Laboratory, Ilmenau University of Technology, Germany. In 1997, he joined Siemens Mobile Networks, Munich, Germany, where he was responsible for strategic research for third generation mobile radio systems. From 1998 to 2001, he was the Director for International Projects and University Cooperation's in the mobile infrastructure business of Siemens in Munich, where his work focused on mobile communications beyond the third generation. He has received the 2009 Best Paper Award from the IEEE Signal Processing Society, the Vodafone Innovations Award for outstanding research in mobile communications, the ITG Best Paper Award from the Association of Electrical Engineering, Electronics, and Information Technology (VDE), and the Rohde & Schwarz Outstanding Dissertation Award. His research interests include wireless communications, array signal processing, high-resolution parameter estimation, and tensor-based signal processing. He has been serving as a Senior Editor for IEEE JOURNAL OF SELECTED TOPICS IN SIGNAL PROCESSING since 2019, an Associate Editor for IEEE TRANSACTIONS ON SIGNAL PROCESSING from 2002 to 2006 and from 2011 to 2015, IEEE SIGNAL PROCESSING LETTERS from 2006 to 2010, the *Research Letters in Signal Processing* from 2007 to 2009, the *Journal of Electrical and Computer Engineering* (Hindawi) since 2009, and the *EURASIP Journal on Advances in Signal Processing* journal from 2011 to 2014, and a Guest Editor for the *EURASIP Journal on Wireless Communications and Networking*. From 2011 to 2019, he was an elected member of the Sensor Array and Multichannel (SAM) Technical Committee of the IEEE Signal Processing Society, where he served as the Vice Chair from 2015 to 2016, the Chair from 2017 to 2018, and the Past Chair in 2019. Since 2020, he has been an elected member of the Signal Processing Theory and Methods (SPTM) Technical Committee of the IEEE Signal Processing Society. Moreover, he has served as the Technical Co-Chair of PIMRC 2005 in Berlin, Germany, ISWCS 2010 in York, U.K., the European Wireless 2014 in Barcelona, Spain, the Asilomar Conference on Signals, Systems, and Computers 2018, USA, and ISWCS 2024 in Rio de Janeiro. He has served as the General Co-Chair of WSA 2013 in Stuttgart, Germany, ISWCS 2013 in Ilmenau, Germany, CAMSAP 2013 in Saint Martin, French Antilles, WSA 2015 in Ilmenau, SAM 2016 in Rio de Janeiro, Brazil, CAMSAP 2017 in Curacao, Dutch Antilles, SAM 2020 in Hangzhou, China, the Asilomar Conference on Signals, Systems, and Computers 2021, USA, and CAMSAP 2023 in Costa Rica.

Xiu Yin Zhang (Fellow, IEEE) received the B.S. degree in communication engineering from the Chongqing University of Posts and Telecommunications, Chongqing, China, in 2001, the M.S. degree in electronic engineering from the South China University of Technology (SCUT), Guangzhou, China, in 2006, and the Ph.D. degree in electronic engineering from the City University of Hong Kong, Hong Kong, China, in 2009. From 2001 to 2003, he was with ZTE Corporation, Shenzhen, China. He was a Research Assistant from July 2006 to June 2007 and a Research Fellow from September 2009 to February 2010 with the City University of Hong Kong. He is currently a Full Professor and the Vice Dean of the School of Electronic and Information Engineering, SCUT. He also serves as the Director of the Engineering Research Center for Short-Distance Wireless Communications and Network, Ministry of Education. He has authored or coauthored more than 180 internationally refereed journal articles (including more than 100 IEEE TRANSACTIONS) and 90 conference papers. His research interests include antennas, MMIC, RF components and sub-systems, intelligent wireless communications, and sensing. He is a fellow of the Institution of Engineering and Technology (IET). He has served as the general chair/co-chair/technical program committee (TPC) chair/a member and a session organizer/the chair for a number of conferences. He was a recipient of the National Science Foundation for Distinguished Young Scholars of China. He won the first prize of 2015 Guangdong Provincial Natural Science Award and the 2020 Guangdong Provincial Technological Invention Award. He was a Supervisor of several conference best paper award winners. He is an Associate Editor of IEEE ANTENNAS AND WIRELESS PROPAGATION LETTERS, *IEEE Antennas and Propagation Magazine*, and IEEE OPEN JOURNAL OF ANTENNAS AND PROPAGATION.